Catalysis Science & Technology

ROYAL SOCIETY OF CHEMISTRY

PAPER

View Article Online
View Journal | View Issue

Cite this: *Catal. Sci. Technol.*, 2021, **11**, 2908

Au-Modified Pd catalyst exhibits improved activity and stability for NO direct decomposition

Taha Elgayyar, †[a] Josefine Schnee, †[b] Alain Tuel, [a] Laurence Burel,[a] Francoise Bosselet,[a] Yves Schuurman, [a] Frederic C. Meunier, *[a] Laurent Delannoy[b] and Cyril Thomas [b]

Received 17th February 2021,
Accepted 25th February 2021

DOI: 10.1039/d1cy00301a

rsc.li/catalysis

The direct decomposition of NO_x at moderate temperatures is a challenge because of the poisoning of the surface of noble metals by oxygen, yet the modification of Pd with Au enables obtaining a highly stable catalyst under an O_2-free feed at 450 °C. Care was taken to ensure that the reaction was not due to the reduction of NO_x with carbonaceous residues by monitoring CO_2 evolution. Pd–Au alloyed domains with a wide range of compositions were evidenced by *in situ* and *ex situ* XRD, the Pd content of which decreased with the increasing oxidising nature of the feed due to phase segregation giving rise to PdO and an Au-rich alloy. Under air, the limiting alloy composition was $Pd_{0.2}Au_{0.8}$. The catalyst was yet inactive in the presence of 5% O_2.

The proportion of vehicles using internal combustion engines will remain significant in the foreseeable future and the drive to reduce CO_2 emissions will favor the use of diesel and lean-burn engines. Yet, these engines exhibit significant drawbacks due to the emissions of NO_x, particulate matters and organic pollutants (*e.g.* unburnt hydrocarbons and formaldehyde, notably present when using natural gas as fuel).[1] The corresponding emission control technologies[2] are complex, *e.g.* NO_x-storage–reduction,[3,4] NH_3-selective catalytic reduction[5,6] and traps for cold starts.[7,8] The formation of highly toxic HCN was even reported, formed from NH_3 and formaldehyde, molecules that are typically present in the exhaust gases of NH_3-SCR system fitted to natural gas engines.[9]

NO decomposition to N_2 and O_2 is strongly favoured below 450 °C, as the equilibrium concentration of NO_x (= NO + NO_2 + N_2O) is lower than 1 ppm when starting with a reaction mixture comprising 200 ppm NO + 10% O_2 in N_2 (Fig. 1). An efficient emission control technology would incorporate first an oxidising converter to combust all organic compounds followed by a NO_x decomposing element that would not require any reducing agent and operate in the presence of O_2. Unfortunately, NO_x direct decomposition is a slow reaction at low temperatures and no catalytic system has yet proven worthwhile of commercial application.

Cu-ZSM-5 exhibits interesting activity for NO decomposition between 300–600 °C, even in the presence of 10% O_2, yet the rates are too low to be of practical interest[10,11] and it is strongly poisoned by SO_x.[12] NO decomposition can be carried out on perovskites, but only at reaction temperatures higher than 600 °C.[10,13]

Many metals and oxides catalyse NO decomposition, but O_2 inhibits the reaction through competitive adsorption.[10,14] In addition, noble metals can become poisoned through extensive oxidation leading to the formation of a less active oxidic phase.[15] This led to the interest in selective catalytic reduction (SCR) of NO_x with hydrocarbons in which oxygen atoms strongly bound to the noble metal could be removed by forming CO_2 and water,[10,16] though this method only led to limited practical applications in the case of heavy-duty engines.[17]

Another approach was proposed by Toyota researchers consisting in Au- and Ir-modifications of Pt/alumina to

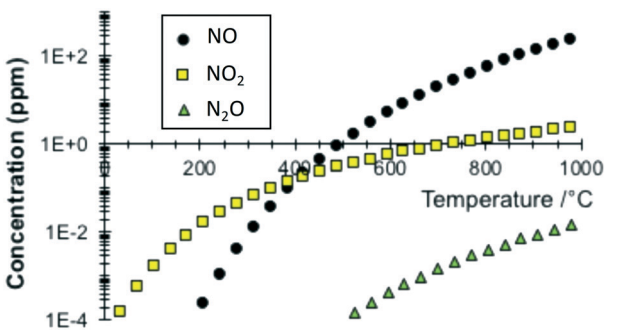

Fig. 1 Thermodynamic equilibrium concentrations of NO, NO_2 and N_2O in a system initially containing 200 ppm of NO and 10% O_2 in N_2 at a total pressure of 1 bar. The much larger equilibrium concentrations of N_2 (*ca.* 90%) and O_2 (*ca.* 10%) are not shown. The data were calculated using the HSC Chemistry 6.2 software.

[a] *Univ Lyon, CNRS, Université Claude Bernard Lyon, IRCELYON, 2 Av. Albert Einstein, 69626 Villeurbanne, France. E-mail: fcm@ircelyon.univ-lyon1.fr*
[b] *CNRS, Laboratoire de Réactivité de Surface (LRS), Sorbonne Université, F-75005 Paris, France*
† These authors contributed equally.

facilitate oxygen desorption from Pt.[18] The improved NO decomposition activity obtained was assigned to the better resistance against oxidation brought about by Au. However, the role of individual promoters was not determined since only trimetallics Pt–Au–Ir were studied. Yet, the Au-rich sample appeared totally inactive, pointing out to the inability of Au alone to decompose NO. Bimetallics Ir–Au supported on alumina and dendrimers were reported later,[19] though the activity was only measured in transient modes, making difficult differentiating true catalytic activity and adsorption phenomena, or even the potential reduction of NO_x with residues from organic dendrimers.

Au oxide is among the least stable of metal oxides, as shown by the plots giving the Gibbs energy of decomposition of various oxides of noble metals (active for NO decomposition) over the temperature range of interest and in the presence of 10% O_2 (Fig. 2).

This observation led us to consider alloys based on Au and Pd, since (i) these metals are fully miscible (in contrast to Au and Pt), (ii) Pd is active for NO decomposition[10] and (iii) Au should facilitate oxygen desorption as suggested earlier.[18] Au was already proposed to protect Pd against oxidation by oxygen,[20] sulfur[20] and chloride[21] through geometric (*e.g.* Pd site dilution) and electronic (*e.g.* electronic transfer from Au to Pd) effects, when used for hydrodechlorination or hydrodesulfurization.

Facilitating oxygen release from Pd at moderate temperature is a challenge, as the heat of adsorption of O atoms on metallic Pd is high (*i.e.* 364 kJ mol^{-1}).[22] Reddy *et al.*[23] reported on the nature and activity of Pd phases during NO decomposition over silica-supported catalysts. NO decomposition was found to be mostly stoichiometric (*i.e.* non-catalytic) at temperatures lower than 500 °C, by which metallic Pd was converted into inert PdO. PdO was shown to decompose significantly to metallic Pd and O_2 only above *ca.* 500 °C, temperature above which truly catalytic NO decomposition could occur.

The support used here was a commercial silica (surface area of 275 m^2 g^{-1}), which was first functionalized by grafting APTMS (3-amino-propyltrimethoxysilane) according to a method reported elsewhere.[24] The two monometallic catalysts were prepared using wet impregnation.[25] The metal precursors were $HAuCl_4{\cdot}3H_2O$ and $Pd(NO_3)_2{\cdot}xH_2O$, both from Aldrich. The metals were reduced with $NaBH_4$ at room temperature. The bimetallic catalyst was prepared using the same batch of the monometallic Pd catalyst. Au was deposited on Pd using a surface redox method[26] by which Au was reduced over the Pd/silica suspension in water in which H_2 was bubbled at room temperature. The final suspension was filtered and washed several times with distilled water and then kept in an oven overnight at 90 °C. After the preparation, the catalysts were kept in a refrigerator in the dark to avoid any sintering or ageing effects on the Au-based particles.

The metal loadings were determined by ICP analyses. The parent Pd/SiO_2 comprised 4.3 ± 0.3 wt% of Pd and the bimetallic had a composition of 4.7 ± 0.3 wt% Pd + 1.0 ± 0.2 wt% Au/SiO_2. The loading of the reference Au/SiO_2 was 1.0 ± 0.2 wt%. The TEM analysis (using a Jeol 2010 LaB6) of the Au/SiO_2 revealed particle sizes comprised between 2 and 9 nm and a surface-weighted diameter d_{sw} ($= \Sigma n_i d_i^3/\Sigma n_i d_i^2$) of 4.7 nm (Fig. 3, top). The parent Pd/SiO_2 showed particle sizes ranging mostly from 2 to 5 nm and a few larger particles up to 14 nm (Fig. 3, middle) and the d_{sw} was 9.1 nm. The bimetallic catalyst exhibited a similar particle size

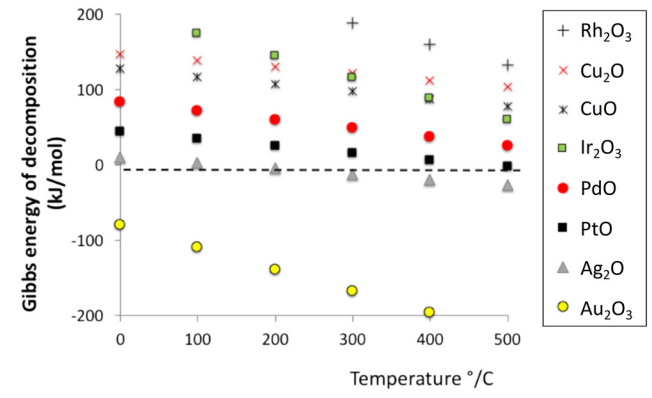

Fig. 2 Gibbs energy of decomposition $M_xO_y \rightarrow x\ M + y/2\ O_2$ for several bulk metal oxides (in equilibrium with 10 kPa of O_2). Data calculated using the HSC Chemistry 6.2 software.

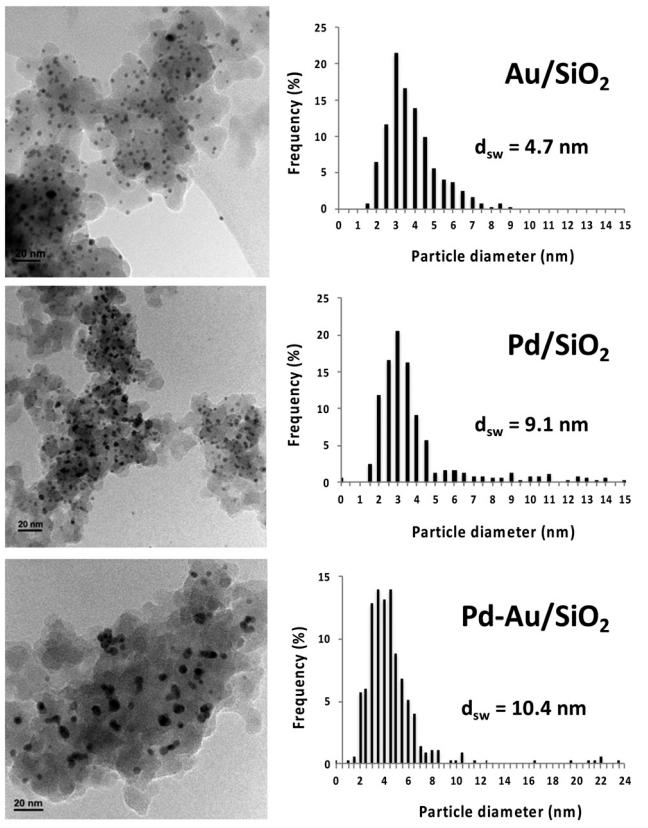

Fig. 3 TEM and particle size distributions of (top) Au/SiO_2, (middle) Pd/SiO_2 and (bottom) $Pd–Au/SiO_2$. The samples were calcined in flowing air at 500 °C and then reduced with H_2 at 450 °C. More than 350 particles were counted for each sample.

distribution, with a few larger particles up to 24 nm, and d_{sw} = 10.4 nm (Fig. 3, bottom).

TEM-EDX microanalyses were carried out over 20 nanoparticles of two aliquots of the 4.7 wt% Pd- 1.0 wt% Au bimetallic catalyst, one aliquot being calcined and then reduced by $NaBH_4$ at room temperature and the second aliquot being calcined and reduced by H_2 at 450 °C. These TEM-EDX analyses cannot be taken as being fully representative of the bimetallic catalyst due to the limited number of particles probed, yet those showed that the composition varied significantly from one particle to another in terms of Au and Pd proportions (Fig. 4). This indicates that the two metals were not homogeneously distributed over the sample, though most nanoparticles (about 90%) were bimetallic.

An *in situ* XRD analysis was carried out using an AntonPaar XRK900 reaction chamber fitted in a Bruker D8Advance. The thermal treatment consisted first of a calcination at 500 °C in a synthetic air flow, followed by a reduction in a H_2 stream at 450 °C, before returning to 25 °C under H_2 and finally air. The pattern of the SiO_2 support was subtracted.

The XRD patterns measured over the Au/SiO_2 (Fig. 5A) were essentially featureless, in agreement with the small Au particle sizes measured by TEM. A broad peak at *ca.* 38° corresponding to metallic Au was observed that hardly evolved with the thermal treatment (Fig. 5A.a to f).

In contrast, the Pd/SiO_2 patterns (Fig. 5B) exhibited strong peaks that evolved depending on temperature and the composition of the feed. The sample was poorly crystallised just after synthesis (Fig. 5B.a), but then exhibited a well-crystallised PdO pattern after calcination at 500 °C (Fig. 5B.b). The mere contact with H_2 at 25 °C led to the reduction of the PdO and the formation of a bulk hydride Pd_2H phase (Fig. 5B.c). The Pd_2H was decomposed by raising the temperature to 450 °C in H_2 and metallic Pd was formed (Fig. 5B.d, the offset from the Pd PDF file line is

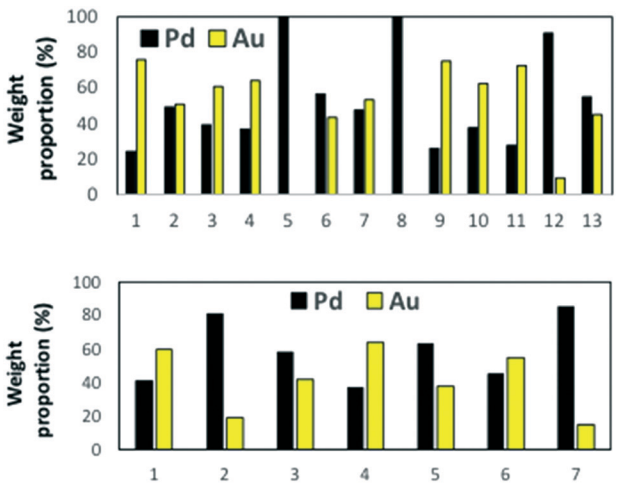

Fig. 4 Proportion (in wt%) of Pd and Au measured by TEM-EDX over the SiO_2-supported bimetallic sample on various nanoparticles (top) calcined at 500 °C and reduced by $NaBH_4$ at room temperature and (bottom) calcined at 500 °C and then reduced with H_2 at 450 °C.

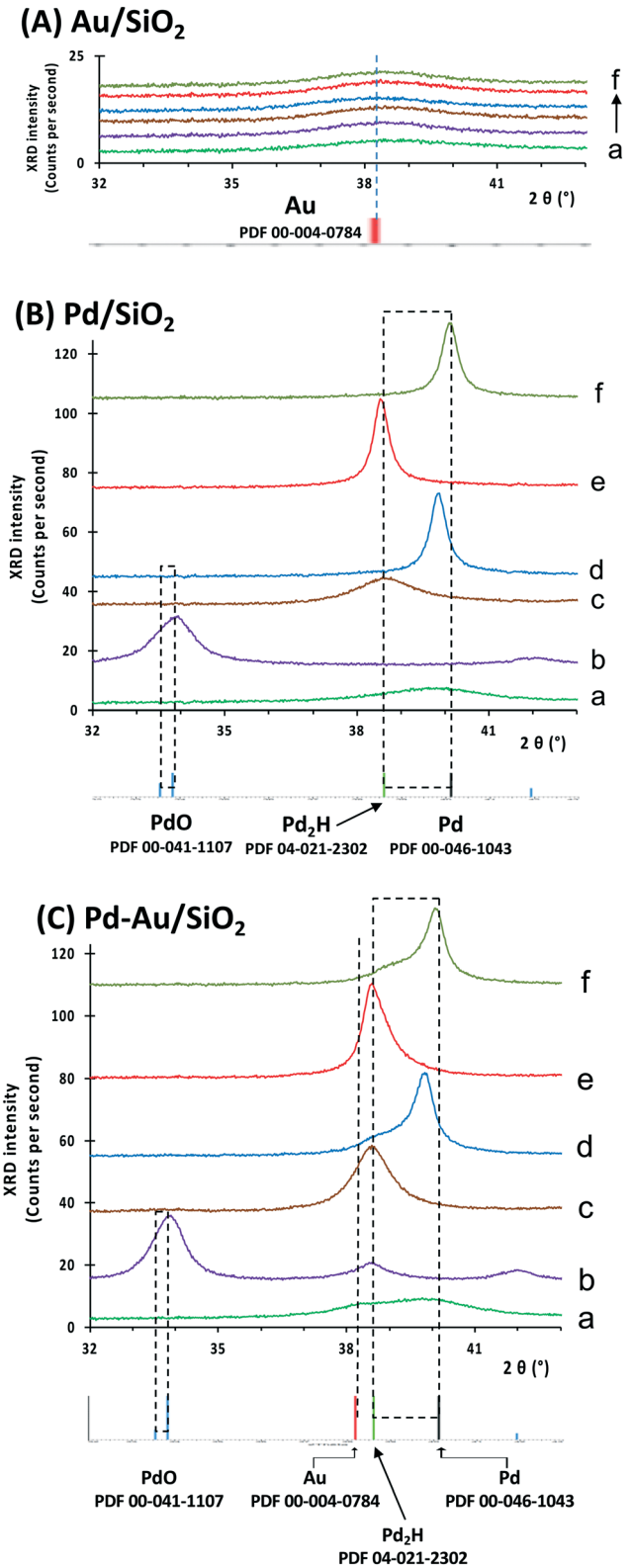

Fig. 5 *In situ* X-ray diffraction patterns of the SiO_2-supported (A) Au, (B) Pd and (C) Pd–Au. The patterns were measured successively at (a) 25 °C in air after synthesis, (b) 25 °C in air after oxidation at 500 °C, (c) 25 °C in H_2, (d) 450 °C in H_2, (e) 25 °C in H_2 and (f) 25 °C in air. The patterns were offset for the sake of clarity. The dotted lines indicate the positions associated with the corresponding ICDD powder diffraction files.

exactly due to the thermal expansion of the lattice parameter from 25 °C to 450 °C). The Pd_2H phase reformed when going back to 25 °C (Fig. 5B.e), but the peak width was narrower, indicating that the thermal treatment had increased the size of the crystalline domains. The hydride phase decomposed upon H_2 being replaced with N_2 then air at 25 °C leading to metallic Pd peak (Fig. 5B.f), probably covered with chemisorbed oxygen.

The XRD results obtained on the Pd/SiO_2 stress that the reduction of PdO is fast, even at 25 °C, once the sample is exposed to H_2. In contrast, the oxidation of Pd to PdO is slow and requires a high temperature calcination. The latter observation is consistent with earlier reports that Pd oxidation to bulk PdO is slow and limited by O diffusion, while O_2 is easily activated at the surface of Pd particles forming chemisorbed O species.[27,28]

The size of the Pd crystalline domains over the Pd/SiO_2 after reduction at 450 °C were determined using Scherrer equation and found to be around 13 nm. This represents the higher range of the particles measured by TEM (Fig. 3, middle), showing that the XRD signal is mostly representative of the (few) larger particles present in the sample.

The analysis of the XRD patterns obtained in the case of the bimetallic Pd–Au sample (Fig. 5C) was complicated by the fact that Au and Pd_2H exhibit a major peak roughly at the same position (*ca.* 38.3°). To make things worse, alloyed phases Pd_xAu_{1-x} are expected to show peaks in between those of Au and Pd. As a consequence, the presence of pure Au can only be assessed whenever no Pd hydride is present, hence at 450 °C or in air. The corresponding $Pd–Au/SiO_2$ patterns (Fig. 5C.b, d and f) did not show any significant contribution at the position corresponding to pure Au, indicating that most gold was poorly crystallised or alloyed with Pd (note that the global molar ratio Pd/Au is about 9).

A large peak at the position of pure Pd (*ca.* 40°) indicated the presence of Pd domains (Fig. 5C.d and f), in agreement with the TEM-EDX data showing the presence of a few pure or Pd-rich particles (Fig. 4). In fact, the nature and evolution of the pattern observed over the bimetallic sample was similar to those observed over the pure Pd/SiO_2, with the exception of broader bands being present at positions in between those of Au and Pd that can be assigned to alloyed phases (compare signals in the dotted boxes in Fig. 5B and C for patterns b, d and f).

Three patterns of the bimetallic sample are shown in Fig. 6 to better highlight the peaks associated with alloyed phases. The pattern obtained after the first calcination at 500 °C exhibited PdO peaks (34° and 42°) and a peak at *ca.* 38.5° (Fig. 6a). The peak at 38.5° correspond to an alloy of composition $Pd_{0.2}Au_{0.8}$ based on Vegard's law. It is interesting to note that this composition corresponds roughly to the limit (*i.e.* $Pd_{0.15}Au_{0.85}$) below which the Pd content of the alloy phase cannot be lowered when oxidising Pd–Au alloy films as those segregate into PdO and an Au-rich alloy phase.[29]

Fig. 6b corresponds to the pattern of the bimetallic Pd–Au sample at 25 °C in air after further reduction at 450 °C in H_2

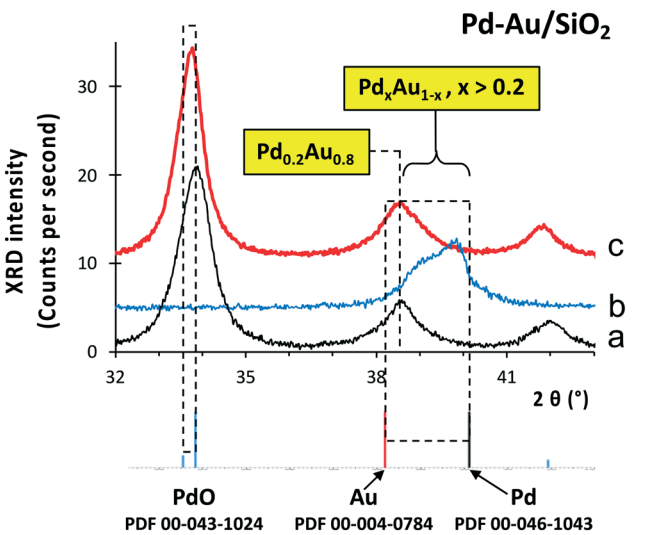

Fig. 6 X-ray diffraction patterns of the $Pd–Au/SiO_2$ at 25 °C in air after successive (a) oxidation at 500 °C, (b) reduction in H_2 at 450 °C and (c) re-oxidation at 450 °C. The pattern (b) was corrected to remove the main contribution of pure Pd domain according to the calculation: pattern (b) = Fig. 5C.f − 0.8 × Fig. 5B.f. The patterns were offset for the sake of clarity.

(Fig. 5C.f) to which the weighted Pd pattern collected in the same conditions (Fig. 5B.f) was subtracted. The obtained pattern revealed the superposition of several peaks comprised between those of pure Au and pure Pd that can be assigned to Pd–Au alloyed phases with various compositions (Fig. 6b). In view of the positions of these peaks, their Pd content appears to be higher than that of the $Pd_{0.2}Au_{0.8}$ phase observed after calcination (20 mol% Pd). This result is again consistent with the TEM-EDX data (Fig. 4) that show a wide range of Pd/Au compositions with many particles being rich in Pd.

A further oxidation of the bimetallic sample led to a pattern (Fig. 6c) that was similar to that collected initially (Fig. 6a) with PdO and an alloyed phase $Pd_{0.2}Au_{0.8}$. This shows the reversibility of the alloying–dealloying process upon reduction–oxidation cycles.

Using the area of the XRD peaks of the Pd and Pd–Au phases for a rough quantitative analysis, the bimetallic sample after reduction contained about 60 wt% of a phase corresponding to pure or almost pure Pd and about 40 wt% of alloyed Pd–Au phases. The quantity of free Au was negligible. It should be reminded at this point that the XRD technique cannot determine whether or not the surface of the "pure" Pd particles would be partly covered with Au atoms. The presence of some Au atoms segregated at the surface can be expected because of the significantly lower surface tension of Au (1145 mJ m^{-2}) as compared to that of Pd (1482 mJ m^{-2}).[30] In addition, we stressed above that the XRD data are mostly representative of the larger nanoparticles present, hence the corresponding compositions and reactivities do not encompass those of the smaller nanoparticles. Nonetheless, these XRD data indicate that a fraction of Pd atoms was made oxidation-resistant by forming an alloy (*i.e.* $Pd_{0.2}Au_{0.8}$) with Au.

The catalytic activity for the decomposition of NO was studied using a setup described in details elsewhere.[31] In brief 100 mg of as-prepared catalyst was placed in a U-shaped quartz reactor on a quartz wool plug. The catalyst was reduced at 200 °C under 50% H_2 in He, before being flushed with He. A reaction flow of 50 mL min^{-1} comprising 500 ppm of NO + 5% O_2 in He was initially used. Reactor effluents were analysed by a combination of μ-gas chromatography (CP490, Agilent), mass spectrometry (Omnistar, Pfeiffer Vacuum) and IR gas cell analyses (MKS MultiGas 2030, MKS). The temperature was raised step-wise to 450 °C.

The evolution of products measured over the non-calcined Pd–Au/SiO_2 revealed significant N_2 and N_2O production, which correlated with the evolution of CO_2 (Fig. 7). This indicates that APTMS residues present at the surface of the silica support were able to react with NO_x and lead to NO_x reduction. This stresses that catalysts should be thoroughly calcined before carrying out NO_x direct decomposition to prevent the risk of unwanted reduction.

The samples were left under 500 ppm NO + 5% O_2 for 10 h at 450 °C to burn off all carbonaceous residues, which was ascertained by the absence of CO_2 in the reactor effluent (Fig. 7). Unfortunately, the activity of the Pd–Au/SiO_2 dropped to zero once CO_2 production ceased, stressing that this catalyst was not active for NO decomposition in the presence of 5% O_2.

The catalysts were then reduced *in situ* under 50% H_2 in He at 450 °C for 1 h to reduce the PdO and ensure the realloying of Pd and Au. The NO decomposition activity of the catalysts was then measured isothermally at 450 °C over 1000 min. O_2 was left out of the feed this time to limit potential fast deactivation due to O-poisoning, as suggested by the initial deactivation observed at 200 °C that was not correlated to the CO_2 signal (Fig. 7).

It is important to note that Au/SiO_2 was essentially not active for NO decomposition reaction under these conditions, as the level of N_2 + N_2O formed (*ca.* 3 ppm) was close to the precision of the measure (Fig. 8, top). Interestingly, the Au-promoted Pd sample appeared significantly more active than the parent Pd/SiO_2 sample, indicating that a synergy existed between these two metals (Fig. 8, top).

In addition, the bimetallic sample activity was stable over the duration of the experiment (following a fast but limited initial deactivation), while that of the monometallic parent sample was continuously decaying. The concentrations of O_2 and NO_2 released during the reaction showed that the release of oxygen was significantly greater in the case of the bimetallic sample (Fig. 9). These observations support the conclusions derived from the XRD data that Au induced a greater resistance against oxidation of at least a fraction of the Pd atoms, which may explain the stability of the Au-promoted Pd catalyst.

The selectivity to N_2 measured over these three catalysts is reported in Fig. 8, bottom. (Note: the complement to 100% represents the selectivity to N_2O, NO_2 being not considered as a reduction product). The high selectivity to N_2 measured over Au/SiO_2 should be taken with caution in view of the low

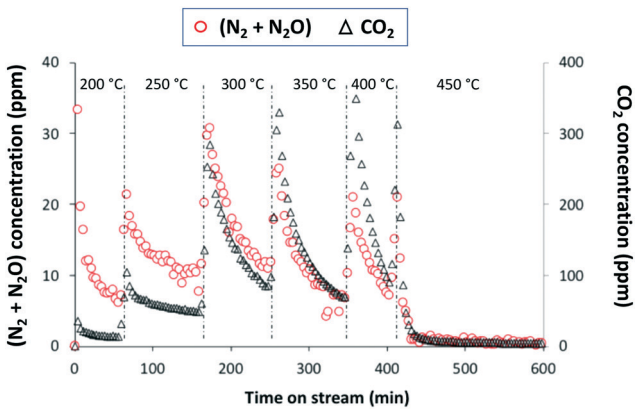

Fig. 7 Product formation recorded over the fresh Pd–Au/SiO_2 under a feed of 500 ppm NO + 5% O_2 in He. The CO_2 observed was produced from the combustion of carbonaceous materials present at the surface of the silica.

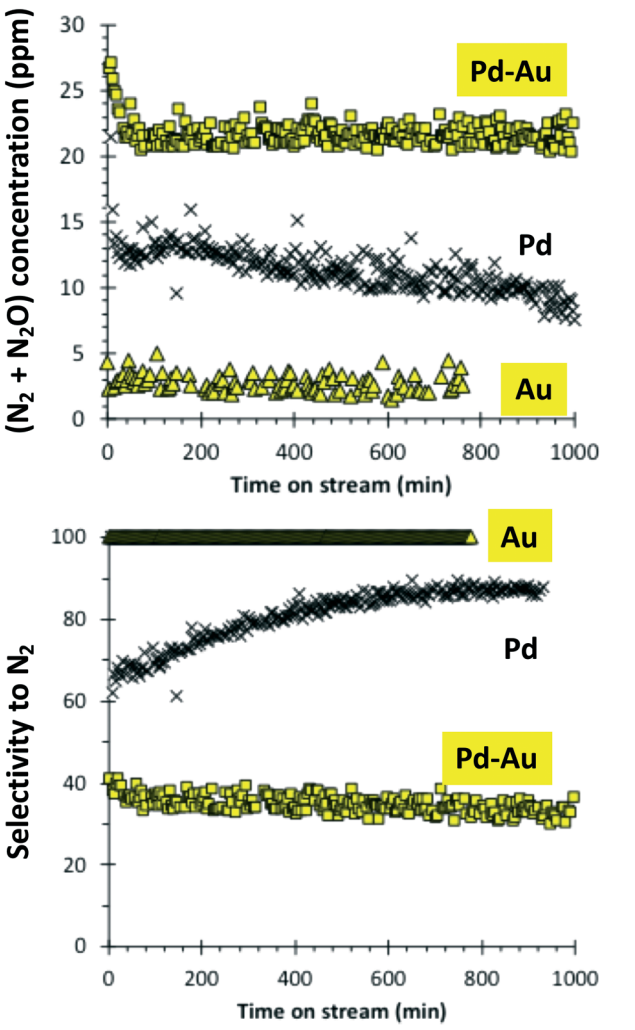

Fig. 8 Decomposition product formation recorded over the (O_2 + NO)-cleaned Au/SiO_2, Pd/SiO_2 and Pd–Au/SiO_2 and subsequently reduced at 450 °C. (Top) concentration of (N_2 + N_2O) and (bottom) selectivity to N_2 (the selectivity to N_2O is the complement to 100%). Reaction temperature: 450 °C. Feed: 500 ppm NO in He.

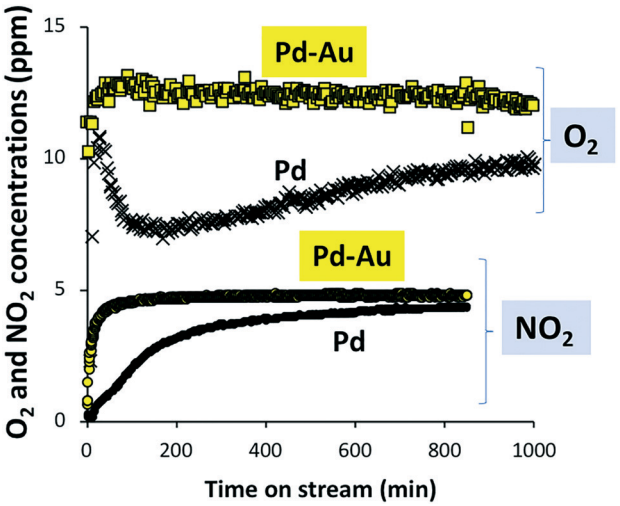

Fig. 9 O_2 and NO_2 concentrations recorded over the (O_2 + NO)-cleaned Pd/SiO_2 and Pd–Au/SiO_2 and subsequently reduced at 450 °C. Reaction temperature: 450 °C. Feed: 500 ppm NO in He.

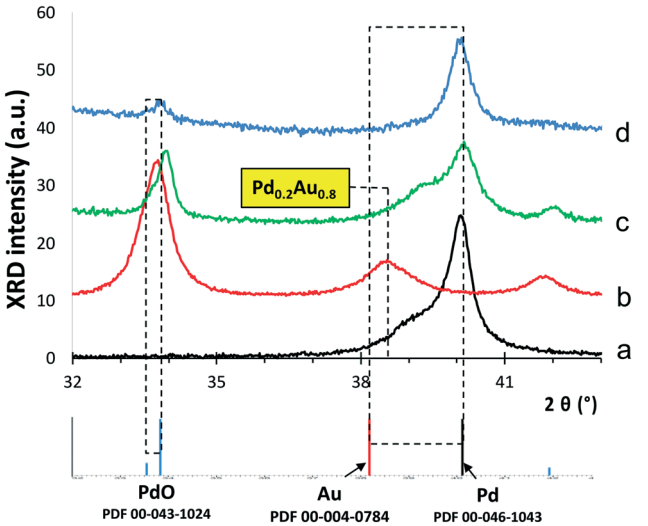

Fig. 10 X-ray diffraction patterns of the Pd–Au/SiO_2 at room temperature in air after (a) reduction in H_2 at 450 °C, (b) oxidation at 450 °C and (c) use for NO decomposition at 450 °C. (d) X-ray diffraction patterns of the Pd/SiO_2 at room temperature in air after use for NO decomposition. The spectra were offset for the sake of clarity.

activity of this sample (part of the N_2 measured may be the results of minute leaks). The Pd/SiO_2 sample showed a rising selectivity to N_2 nearing 90%, while that of the Pd–Au/SiO_2 remained essentially constant at 35%. This significant selectivity difference suggests that the Pd active sites were modified by Au, likely through the dilution of the Pd centres that may have induced both geometric and electronic effects.

As reported in the literature[29,32–34] and shown in Fig. 6, heating Pd–Au alloys in O_2 above 450 °C results in the formation of partially oxidised Pd (or even PdO) at the alloy surface and segregation. Similarly, a fraction of the Pd in the Pd–Au alloyed nanoparticles may have eventually got segregated under NO, a strong oxidizer. The XRD of the bimetallic sample was collected after the NO decomposition reaction shown in Fig. 8 and 9. Interestingly, the pattern obtained after NO decomposition at 450 °C exhibited peaks of PdO, alloyed phases Pd_xAu_{1-x} and Pd (Fig. 10c). This pattern is therefore intermediate between that obtained after reduction at 450 °C showing Pd_xAu_{1-x} and Pd (Fig. 10a) and that obtained after calcination at 450 °C showing PdO and $Pd_{0.2}Au_{0.8}$ (Fig. 10b). This can be simply rationalised by the fact that 500 ppm of NO has a lower oxidising potential than air.

The presence of PdO, Pd and Pd_xAu_{1-x} post-reaction stresses the complex speciation of Pd existing over the bimetallic catalyst, due to the wide range of particle sizes and composition existing in the as-prepared sample (Fig. 3 and 4). It is therefore difficult to infer on the nature of the most active and stable phase. Surprisingly, the Pd/SiO_2 post-reaction exhibited an almost negligible fraction of PdO (Fig. 10d), in contrast to the bimetallic sample (Fig. 10c). This observation can possibly be explained by an improved diffusion of O in the alloyed domains (presenting more defects), as O diffusion has been proposed as the limiting step during Pd oxidation.[27,28]

The stability of the bimetallic sample during NO decomposition (Fig. 8, top) indicates yet that under our reactions conditions most bimetallic nanoparticles exhibited a sufficient Au fraction at the surface to prevent deactivation, in agreement with the TEM-EDX analysis (Fig. 4). The XRD analysis was yet unable to capture this nanoscale insight by pointing out a large fraction of seemingly pure Pd domains, which may have actually been superficially covered with Au. Again, the XRD analysis is likely to have overemphasized the signal of larger particles that are less important for catalysis.

In situ characterization methods would need to be employed to determine the nature of the active surface, since surface segregation is likely to occur when altering the atmosphere composition, even at room temperature, as reported in the case of CO adsorption over Au–Pd and other nanoalloys.[35,36] We have carried out *operando* DRIFTS analyses to try to monitor NO_x species adsorbed on the catalyst under reaction conditions at 450 °C, but no meaningful signal could be obtained (data not shown).

In conclusion, catalysts should be free of carbonaceous deposits when investigating NO decomposition, as the unexpected presence of potential reductants (or using carbonaceous supports) could be a cause of data misinterpretation. Monitoring CO_2 production can help in assessing this point, as demonstrated here (Fig. 7). The addition of Au does promote the activity of Pd/SiO_2 leading to a more active catalyst that exhibited a stable activity under our reaction conditions over more than 16 h. This raises the prospect of developing better oxidation-resistant catalysts based on noble metals and Au for the direct decomposition of NO. The effect of water will be important to investigate because it is known to deactivate Pd-based catalysts used for methane oxidation by forming strongly bound surface hydroxyls.[37] Water can also facilitate sintering.

Since the activity for NO decomposition in the presence of 5% O_2 was essentially nil (Fig. 7), other formulations (possibly based on metals other than Pd) will have to be considered for practical applications in the presence of large O_2 concentrations. Formulations based on Pt or Ag alloyed to Au are currently being investigated, following the insights given by the thermodynamics of oxide decomposition reported in Fig. 2. Another challenge will be to retain activity in the presence of SO_x.

Author contributions

FCM designed the project, carried out the thermodynamic analysis, monitored the data and drafted the manuscript. TE carried out the catalyst synthesis and participated to the literature review and data analysis. LB carried out the TEM-EDX analysis. FB carried out the XRD analysis. AT and YS contributed to data analysis and manuscript writing. JS carried out the NO decomposition experiments, data analysis and reviewed the manuscript. LD provided support in the synthesis of the catalysts and reviewed the manuscript. CT built and validated the catalytic set-up, monitored the catalytic results and reviewed the manuscript.

Conflicts of interest

There are no conflicts to declare.

Acknowledgements

TE and JS acknowledge funding from the ANR project DECOMPNOx (ANR-18-CE07-0002-01).

Notes and references

1 T. W. Hesterberg, C. A. Lapin and W. B. Bunn, *Environ. Sci. Technol.*, 2008, **42**, 6437–6445.
2 M. V. Twigg, *Catal. Today*, 2011, **163**, 33–41.
3 N. Takahashi, H. Shinjoh, T. Iijima, T. Suzuki, K. Yamazaki, K. Yokota, H. Suzuki, N. Miyoshi, S. Matsumoto, T. Tanizawa, T. Tanaka, S. Tateishi and K. Kasahara, *Catal. Today*, 1996, **27**, 63–69.
4 J. P. Breen, C. Rioche, R. Burch, C. Hardacre and F. C. Meunier, *Appl. Catal., B*, 2007, **72**, 178–186.
5 X. Ye, J. E. Schmidt, R.-P. Wang, I. K. van Ravenhorst, R. Oord, T. Chen, F. de Groot, F. Meirer and B. M. Weckhuysen, *Angew. Chem.*, 2020, **59**, 15610–15617.
6 A. M. Beale, F. Gao, I. Lezcano-Gonzalez, C. H. F. Peden and J. Szanyi, *Chem. Soc. Rev.*, 2015, **44**, 7371–7405.
7 Y. Murata, T. Morita, K. Wada and H. Ohno, *SAE Int. J. Fuels Lubr.*, 2015, **8**, 454–459, DOI: 10.4271/2015-01-1002.
8 K. Khivantsev, N. R. Jaegers, L. Kovarik, J. C. Hanson, F. Tao, Y. Tang, X. Zhang, I. Z. Koleva, H. A. Aleksandrov, G. N. Vayssilov, Y. Wang, F. Gao and J. Szanyi, *Angew. Chem., Int. Ed.*, 2018, **57**, 16672–16677.
9 D. Zengel, P. Koch, B. Torkashvand, J.-D. Grunwaldt, M. Casapu and O. Deutschmann, *Angew. Chem.*, 2020, **59**, 14423.
10 M. Iwamoto and H. Hamada, *Catal. Today*, 1991, **10**, 57–71.
11 T. C. Peck, G. K. Reddy and C. A. Roberts, *Catal. Sci. Technol.*, 2019, **9**, 1132–1140.
12 M. Iwamoto, H. Yahiro, S. Shundo, Y. Yoshihiro and N. Mizuno, *Appl. Catal.*, 1991, **69**, L15–L19.
13 H. Iwakuni, Y. Shinmyou, H. Yano, H. Matsumoto and T. Ishihara, *Appl. Catal., B*, 2007, **74**, 299–306.
14 A. Amirnazmi, J. E. Benson and M. Boudart, *J. Catal.*, 1973, **30**, 55–65.
15 A. Amirnazmi and M. Boudart, *J. Catal.*, 1975, **39**, 383–394.
16 R. Burch, J. P. Breen and F. C. Meunier, *Appl. Catal., B*, 2002, **39**, 283–303.
17 World patent assigned to Tenneco, WO2013019419A3, 2013-03-28, "Exhaust Treatment System With Hydrocarbons Lean NOx Catalysts".
18 A. Morikawa, K. Okumura, M. Ishii, K. Kikuta, A. Suda and H. Shinjo, *Rare Met.*, 2011, **30**, 53–57.
19 Y.-J. Song, Y. M. López-De Jesús, P. T. Fanson and C. T. Williams, *Appl. Catal., B*, 2014, **154–155**, 62–72.
20 A. M. Venezia, V. La Parola, V. Nicoli and G. Deganello, *J. Catal.*, 2002, **212**, 56–62.
21 S. Karanjit, A. Jinasan, E. Samsook, R. N. Dhital, K. Motomiya, Y. Sato, K. Tohji and H. Sakurai, *Chem. Commun.*, 2015, **51**, 12724–12727.
22 A. N. Salanov and E. A. Suprun, *Kinet. Catal.*, 2009, **50**, 31–39.
23 G. K. Reddy, C. Ling, T. C. Peck and H. Jia, *RSC Adv.*, 2017, **7**, 19645–19655.
24 C.-H. Tu, A.-Q. Wang, M.-Y. Zheng, X.-D. Wang and T. Zhang, *Appl. Catal., A*, 2006, **297**, 40–47.
25 G. X. Pei, X. Y. Liu, A. Wang, L. Li, Y. Huang, T. Zhang, J. W. Lee, B. W. L. Jang and C.-Y. Mou, *New J. Chem.*, 2014, **38**, 2043–2051.
26 F. Gauthard, F. Epron and J. Barbier, *J. Catal.*, 2003, **220**, 182–191.
27 R. Burch, *Catal. Today*, 1997, **35**, 27–36.
28 E. H. Voogt, A. J. M. Mens, O. L. J. Gijzeman and J. W. Gues, *Surf. Sci.*, 1997, **373**, 210–220.
29 L. Hilaire, P. Legare, Y. Holl and G. Maire, *Surf. Sci.*, 1981, **103**, 125–140.
30 B. J. Keene, *Int. Mater. Rev.*, 1993, **38**, 157–192.
31 J. Schnee, L. Delannoy, G. Costentin and C. Thomas, *J. Phys. Chem. C*, 2020, **124**, 22459–22470.
32 R. Ferrando, J. Jellinek and R. L. Johnston, *Chem. Rev.*, 2008, **108**, 845–910.
33 J. K. Edwards, B. E. Solsona, P. Landon, A. F. Carley, A. Herzing, C. J. Kiely and G. J. Hutchings, *J. Catal.*, 2005, **236**, 69–79.
34 D. I. Enache, J. K. Edwards, P. Landon, B. Solsona-Espriu, A. F. Carley, A. A. Herzing, M. Watanabe, C. J. Kiely, D. W. Knight and G. J. Hutchings, *Science*, 2006, **311**, 362–365.
35 B. Zhu, G. Thrimurthulu, L. Delannoy, C. Louis, C. Mottet, J. Creuze, B. Legrand and H. Guesmi, *J. Catal.*, 2013, **308**, 272–281.
36 T. Elgayyar, R. Atwi, A. Tuel and F. C. Meunier, *Catal. Today*, DOI: 10.1016/j.cattod.2021.01.009, in press.
37 R. Burch, D. J. Crittle and M. J. Hayes, *Catal. Today*, 1999, **47**, 229–234.

